RSC Advances

ROYAL SOCIETY OF CHEMISTRY

www.rsc.org/advances

Influence of Interface Properties on Charge Density, Band Edge Shifts, and kinetics of Photoelectrochemical Process in p-Type NiO Photocathode

Qian Liu [a], Lifang Wei [a], Shuai Yuan [a], Xin Ren [a], Yin Zhao *[a], Zhuyi Wang [a], Meihong Zhang [a], Liyi Shi *[a], Dongdong Li [b], Aijun Li [c]

[a] Research Center of Nanoscience and Nanotechnology, Shanghai University, 99 Shangda Road, Shanghai 200444, China

[b] Division of Energy and Environment Research, Shanghai Advanced Research Institute, Chinese Academy of Sciences, Shanghai 201203, China

[c] School of Materials, Shanghai University, 99 Shangda Road, Shanghai 200444, China

E-mail: zhaoyin@shu.edu.cn; shiliyi@shu.edu.cn

Abstract

Nickel oxide as one of few p-type semiconductors exhibits great potential application in construction of photovoltaics and solar fuel production devices. The present work focuses on understanding the surface structure of NiO with controlled surface Ni^{3+} species (e.g. NiO(OH) structure) that accompany the electrochemical processes in NiO/liquid electrolyte interfaces. By the aid of Mott-Schottky method, electrochemical impedance spectroscopy and photocurrent-voltage correlation testing,

the variety of NiO surface structure are correlated to the observed changes in band energies, energetic distribution of the trap states density, charge interface transfer, charge transport, and as result p-type DSSCs device performance. The primary results demonstrate NiO(OH) species act as recombination center and cause worse interface recombination. Furthermore, we also offer an effective way of reducing surface NiO(OH) structure by $Ni(CH_3COOH)_2$ post-treatment method, resulting in 31.3% increased photovoltaic performance. Our work provides good guidance for design and fabrication of solar energy-related devices employing NiO electrode.

Keywords: NiO photocathode, interface, photoelectrochemical, p-type DSSCs

1. Introduction

Recently, p-type oxide semiconductors have become a more active field of research, as p-type oxide cathodes integrating with n-type oxide anodes to produce tandem photovoltaic devices, will improve the performance and reduce the cost of solar harvesting system[1, 2]. Nickel oxide (NiO) is a promising candidate for wide band gap p-type semiconductors[3]. Usually, NiO is a non-stoichiometric crystal which reveals p-type characteristics by hole transport originated from nickel vacancies and/or oxygen interstitials[4-7]. Because of this interesting combination of electrical and optical properties, NiO_x has attracted attention as an electrode material for electrochromic window[8, 9], optoelectronic devices[6] ,dye-sensitized solar cells, photoelectrochemical

water splitting[10, 11] and photoelectrochemical producting chemical fuels[12].

Be similar with the n-type solar energy-related device, the essential processes of photogeneration, separation and recombination of charge carriers all occur primarily in the heterointerface, such as NiO/organic photoactive layer (NiO/P3HT)[13], NiO/organic emitting layer (NiO/CBP and Ir-$(mppy)_3$)[6], NiO/organic-inorganic hybrid photoactive layer (NiO/$CH_3NH_3PbI_3$)[14] or NiO/liquid electrolyte (NiO/acetonitrile, NiO/water et al.). Thus the interfacial energetics and kinetics of these heterointerface are of paramount importance in determining devices performance[15].

It is known that NiOx materials have complex chemical structure (e.g. NiO, Ni_2O_3), meanwhile, which are susceptible to bond to many types of atmospheric molecules, as well as to form several hydroxide structures (e.g. $Ni(OH)_2$, NiOOH)[6, 16, 17]. Greiner et al. found that the surface properties of NiO can affect organic energy-level alignment in the NiO/organic hole-transport materials (α-NPD) interfaces[18]. Recently, Wang et al. have reported the formation of NiO(OH) at NiO/P3HT interface leads to increase in the work function, resulting in enhanced polymer solar cells performance[19]. Liu et al. found that more nickel oxyhydroxide species existing at NiO/organic emitting layer interface show higher hole injection and organic light-emitting efficiency of organic light-emitting device[20]. However, in electrochemical systems with nanoporous NiO_X/liquid electrolyte interfaces, few researchers studied the chemically resolved surface electronic structure of electrode and its related influence for interfacial energetics, charger carriers transfer and relaxation dynamics, as well as the charge recombination rates.

In this work, our goal is to gain the deeper understanding the nature of NiO surface changes that accompany the electrochemical processes in NiO/liquid electrolyte interfaces. Here we adopted post-treatment such as thermal and UV-ozone method to control NiO structure, meanwhile represents a series of characterizations of NiOx/liquid interfaces, and establishes the relativity between complex surface chemistries of NiO film and its band energies, energetic distribution of the trap states density, charge transfer rates relevant to p-type DSSCs. In addition, investigations of the current density-voltage (J-V) properties and device performance, employing the bare and post-treatment NiO films, help to know the key influence of interface structure on kinetics of photoelectrochemical process occurring in p-type DSSCs, but also clear what kind of surface structure of NiO film can obtain well photovoltaic performance. In the final, we find the surface or interface treatment method to eliminate or passivate the surface defects, resulting in the enhancement of photovoltaic performance.

2. Experimental Section

2.1 Preparation of Bare and Post-treatment NiO Photocathode

A precursor solution of NiO was prepared by mixing $NiCl_2$ (1 g), co-polymer F108 (1 g), Milli-Q water (3 g) and ethanol (6 g) according to the literature[21]. The as-prepared NiO films were made by doctor-blading method on FTO (8 Ω) and dried at room temperature for at least 30 min, followed by sintering in an oven at 450℃ for 30 min,

and repeat three times (sample NiO). To study how the surface changes of NiO film affect the electrochemical processes, three designs were taken into account: i) one more calcination at 450℃ for 30 min (sample NiO-S), ii) putted the NiO film in UV-ozone cleaning machine for 30 min (sample NiO-ozone) and iii) applied the NiO film by soaking in 20 mM $Ni(CH_3COOH)_2$ water solution for 30 min at 70℃, followed by a water rinse and drying at 70°C (sample NiO-Ac). The thickness d of all resulting NiO films are 1.1±0.02 μm and the active area is 5.0 mm × 5.0 mm.

2.2 Fabrication of p-type DSSCs

To study the relativity between complex surface chemistries of NiO photocathode and the kinetics of photoelectrochemical process, the resulting NiO films as photocathodes were assembled into p-type DSSCs. Firstly, the resulting NiO films were allowed to heat to 110℃ for 30 min, before being immersed in a C343 dye solution (0.3 mM in acetonitrile) for 16 h. The counter electrodes were platinized by thermal decomposition of H_2PtCl_6 from isopropanol on an FTO at 450℃ for 30 min. A 60 μm meltonix polymer spacer (Solaronix) was used as the primary sealing material. Then, an electrolyte composed of 1.0 M LiI and 0.1 M I_2 in acetonitrile solvent was injected through the hole predrilled on the counter electrode. The hole then sealed with a glass slide.

2.3 Characterization

Morphology observation photoelectrodes were verified by electron microscopy (SEM)

on JEOL JSM-700F. X-Ray diffraction (XRD) measurements were taken on a Rigaku D/MAX-RB X-ray diffractometer using Cu Kα radiation (40 kV, 20 mA) and a secondary beam graphite monochromator to study the crystal structure of the films. X-ray photoelectron spectroscopy (XPS, Mg K-L3 = 1253.6 eV) was performed in a Perkin-Elmer PHI 5000C ESCA system equipped with a dual X-ray source and a hemispherical energy analyser. Spectra were calibrated in energy using C1s = 284.6 eV as reference, and the resolution was estimated at about 0.9 eV.

The Mott-Schottky (MS) plots of bare NiO and post-treated NiO films were measured in aqueous electrolyte by PGSTAT 128N potentiostat (Switzerland, Autolab). The measurements were carried out in a glass electrolytic cell, in a three-electrode configuration. The electrolyte used was a 0.1 M PB aqueous (solution of 0.2 M sodium dihydrogen phosphate mixed with 0.2 M sodium hydrogen phosphate) with 1 M potassium chloride as supporting electrolyte. The pH of the electrolyte was adjusted to 7.0. The reference electrode was Ag/AgCl in saturated KCl, and a porous graphite stick was used as the counter electrode. Nitrogen was passed for 15 min through the electrolyte to remove any dissolved oxygen.

After the assembly of the cell, the electrochemical impedance was measured with an PGSTAT 128N potentiostat (Switzerland, Autolab) in the frequency range of 1×10^{5} to 1×10^{-1} Hz. The AC amplitude was 10 mV. The working electrode was connected to the NiO electrode, and the counter and reference electrode were connected to the platinized counter electrode. The cells were measured in the dark at various potential. The EIS data was analyzed using Nova software with the transmission line equivalent

circuit. The fitting results and detailed explanation can be found in the Supporting Information. The photovoltaic properties were measured using a Keithley 2400 Source Meter under the irradiation of simulated sunlight (100 mW cm^{-2}) provided by an Oriel Sol 3A Class AAA solar simulator with an AM 1.5 filter.

3. Results and Discussion

3.1 Surface Chemical Structure

X-ray photoemission spectroscopy (XPS) used to characterize various different oxidation states of Ni in NiO film, which probe changes in near surface composition of modified NiO photocathode. Fig. 1 and 2 show the Ni 2p and O 1s XPS spectra of bare and modified NiO film. All samples contain the main peaks in the Ni $2p_{3/2}$ at ~ 853.7 eV and O 1s at ~529.3 eV signals, which are corresponding to the stoichiometric NiO[16, 22-24]. To further investigated the species, the shoulder peaks in the Ni $2p_{3/2}$ signals were fitted with signals from the $Ni(OH)_2$ peaks at ~855.1 eV and NiO(OH) peaks at ~856.0 eV(fitting results given in Fig.1 and Table 1)[24]. As shown in Table 1, the amounts of the NiO(OH) species in NiO film reduced after the additional thermal treatment. Especially, the peaks of the surface Ni^{3+} species (e.g. NiO(OH) species) in the sample NiO-S film are too weak to deconvolute. By compared with the bare NiO film, the Ni 2p spectrum shifts higher binding energy after the UV-ozone treatment. As show in Table 1, the calculated content of NiO(OH) species of sample

NiO-ozone shows obvious increase. Accordingly, the O 1s spectrum (as shown in Fig. 2) of sample NiO-ozone shows dramatically change compared with sample NiO and NiO-S, with the shoulder peak for NiO(OH) component becoming more pronounced[16]. Both of these results prove that the UV-ozone treatment can introduced more dipolar NiO(OH) species on the NiO film surface. Obviously, the post-treatment such as thermal or UV-ozone treatment can influence the surface chemical structure of NiO film, and the effect of these surface chemical structure changes on p-type DSSCs device performance will discuss below.

3.2 Band-edge Movement and Acceptor Density

Further analysis of energy band structure of bare and post-treatment modified NiO film was performed using Mott-Schottky (MS) Equation[25],

$$1/C_{SC}^2 = -2(E_{app} - E_{fb} - k_B T/e)/(e\varepsilon_0 \kappa N_A A^2) \quad (1)$$

where C_{sc}, e, ε_0, κ, E_{app}, E_{fb}, k_B, T, N_A and A are capacitance, the fundamental charge constant, vacuum permittivity, dielectric constant, applied potential bias, flat-band potential, Boltzmann constant, temperature, density of acceptors within the space charge region, effective surface area of the semiconductor, respectively. Plotting $1/C_{sc}^2$ vs applied potential E_{app} enables the estimation of N_A and E_{fb}, as show in Fig. 3 and Table 2. The linear parts of the MS plots reveal flat-band potentials (listed in Table 2) are 0.40, 0.44 and 0.38 V vs NHE for sample NiO, NiO-S and NiO-ozone, respectively. A larger slope represents lower acceptor density (N_A). As show in Table 2, sample NiO-ozone shows highest acceptor density ($N_A = 8.44\times10^{18}/cm^3$), followed

by sample NiO ($N_A = 7.75\times10^{18}/cm^3$) and sample NiO-S ($N_A = 7.56\times10^{18}/cm^3$). Namely, the sample NiO-S demonstrates a positive shift of E_{fb}, compared with the sample NiO, which was attributed to the decreasing the surface states by additional thermal treatment. In the case of sample NiO-ozone, more dipolar nickel oxyhydroxide (NiO(OH)) species added through UV-ozone treatment affect the chemical environment of NiO-solution interface, leading to an obvious negative movement of E_{fb}. Since the E_{fb} associate with the Fermi level of NiO, as a result, the movement of E_{fb} will affect the open circuit of DSSCs [26, 27].

3.3 Charge Transport and Recombination

3.3.1 General Description of Impedance Spectroscopy

To study the relationship between complex surface chemistries of NiO photocathode and the kinetics of photoelectrochemical process occurring in p-type DSSCs, the cells employing the bare and modified NiO photocathode were fabricated. Then, electrochemical impedance spectroscopy (EIS) was carried out in dark at the different bias voltages (V_{app}). Their typical Nyquist and Bode plots are shown in Fig. 4. In the Nyquist plots, two semicircles are clearly visible, a smaller one in the high frequency region corresponding to the charge transfer at the electrolyte/counter electrode interface, a larger one in the low frequency region resulting from the hole transfer at the NiO/dye/electrolyte interface (recombination resistance) and hole transport in the NiO photocathode (hole transport resistance) [28-30]. In the Bode plots, the frequency

peak position related to the charge transfer at NiO/dye/electrolyte interface is shifted. And the peak frequency of the larger semicircle is inversely proportional to the lifetime (τ_h) of hole in a photocathode. The hole lifetime estimated from the expression $\tau_h = 1/2\pi f_{max}$ (f_{max} is the peak frequency) is sample NiO-S>sample NiO>sample NiO-ozone in order. To fit the experimental data, the transmission line model was used and the corresponding parameters obtained by the equivalent circuit are listed in Table S1 and Fig. 5.

3.3.2 Chemical Capacitance and Trap States Distribution

As shown in Fig. 5A, the chemical capacitance (C_μ) exhibits an exponential trend as a function of corrected potential (V_{corr}, the corrected method as shown in SI), which arises from the energetic distribution of the trap states density above the valence band-edge[29, 31]. The depth of the trap energy distribution is governed by the parameter α according to:

$$C_\mu = C_0 \exp(q\alpha V_{corr}/k_B T) \quad (3)$$

Where k_B is the Boltzmann constant, T is the absolute temperature, C_0 is the factor of the exponential increase and q is the elementary charge[32]. α is a parameter that accounts for the depth of the trap energy distribution. As show in Table S2, the fits give α values ranging between 0.02 and 0.05, which are more smaller than those of n-type dye sensitized solar cells for which is reported to range between 0.2 and 0.4[33-35]. Small values of α indicates the broadening of the trap distribution. Thus, the wider and deeper trap states energy distribution of NiO photocathode reveals that the

serious charge recombination problems is dominant factor of the photovoltaic performance[36-38].

3.3.3 Charge Recombination

The interfacial recombination resistance (R_{rec}) at the NiO/dye/electrolyte interface is related with the recombination of the photo-injected hole from the NiO valence band with the reduced species of electrolyte. As shown in Fig. 5B, the R_{rec} of all the cells decreases exponentially with the increase of the corrected voltages (Fig. 5B), due to the increased the hole density in the valence band[39]. It also clearly shows that the cell based on sample NiO-S shows a higher R_{rec} than bare NiO cell at the same external bias. This observed higher R_{rec} of sample NiO-S can be attributed to the decrease of surface defect by addition thermal treatment, which can inhibit hole back transfer from the NiO to electrolyte.

In contrast, the cell employing sample NiO-ozone film revealed relatively lower R_{rec} compared with bare NiO cell. The UV-ozone treatment can introduced more (NiO(OH)) species onto the NiO photocathode surface (supported by XPS results)[16]. Wang et al reported that Ni^{3+} is also an acceptor for electron[40]. Besides, NiO(OH) species have the dipole moment pointing toward the NiO surface. Thus, NiO(OH) species could intensify electron injection from the reduced species of electrolyte into NiO, and then cause the recombination with injected hole in the valence band.

3.3.4. Hole Lifetime, Charge transport time and Collection Efficiency

The hole transport resistance (R_t), transport time (τ_{th}) and hole lifetime (τ_h) of the cells employing the bare and modified NiO photocathode are plotted in Fig. 5B and C as function of corrected bias voltage. Obviously, R_t and τ_{th} for modified NiO DSSCs do not change much with the addition thermal or UV-ozone surface treatment. Significantly, the order of τ_h is sample NiO-S>sample NiO>sample NiO-ozone. Generally, efficient charge collection is a prerequisite for the efficient conversion of light to electrical energy. The collection efficiency (η_{cc}) reflects by the competition between transport and recombination of hole, which are calculated and shown in Fig. 5D and Table S1. It noted that η_{cc} was sample NiO-S>sample NiO>sample NiO-ozone in order.

3.4 Photovoltaic Performance

Fig. 6 and Table S3 show the current-voltage characteristics of p-type DSSCs based on bare and modified NiO photocathode as measured under AM 1.5 irradiation. The reference cell (bare NiO photocathode, sample NiO) produced J_{sc} of 1.18 mA/cm^2, V_{oc} of 74mV, and FF of 37.7, corresponding to η of 0.032%. Additional thermal treatment (sample NiO-S) decreased the J_{sc} to 1.13 mA/cm^2, it was explained by the reduction of dye absorption amount from 4.07 to 3.92×10^{-8} mol/cm^2. It is notable that the additional thermal treatment (sample NiO-S) markedly raises the V_{oc} to 81mV, resulting the η of 0.036%. Apparently, the enhanced efficiency is ascribed to the increased V_{oc}. Based on the EIS analysis, the higher R_{rec} of sample NiO-S, and thus as result of effective hole collection, plays positively role in the V_{oc} of cell. With regard

to the surface modified NiO photocathode by UV-ozone treatment, sample NiO-ozone exhibits obvious decrease in V_{oc} of 66 mV and J_{sc} of 0.72 mA/cm^2, leading to about 37.5% decrease of the η (0.020%) compared with bare NiO photocathode (0.032%). This result can be related to the fact that low R_{rec} of sample NiO-ozone leading to relatively serious interfacial charge recombination, which brings about low J_{sc} and V_{oc}.

Combination of above surface microstructure and photoelectrochemical properties analysis, the surface chemistries of NiO photocathode are considered to determine the interface recombination resistance and play a significant role in the effect on p-type DSSCs device efficiency. Therefore, another important issue is to find an way to modified NiO photocathode with less surface defect species, especially of the NiO(OH) structure, but with less negative effect on other properties such as dye absorption amount and hole transportation et al., which can be predicted to result well photovoltaic performance. In present study, we employed the $Ni(CH_3COOH)_2$ post treatment method to modify NiO photocathode. Compared with the bare NiO photocathode (sample NiO), the $Ni(CH_3COOH)_2$ post treatment method successfully reduce the surface NiO(OH) structure without effect on the crystal structure, morphology and dye absorption ability (supported by XRD, SEM and XPS results, as shown in Fig. S1, S2, S3 and Table S4). Thus, the $Ni(CH_3COOH)_2$ post treatment method could passivate surface defect states and prevents the traps from playing part in the hole back reaction. In the aspects of photovoltaic performance (as shown in Fig. S4 and Table S3), the cell employing $Ni(CH_3COOH)_2$ surface modified NiO

photocathode exhibits an obvious increase in V_{oc} to 80 mV and J_{sc} to 1.45 mA/cm^2, which lead to the cell efficiency to reach $\eta = 0.042\%$ (Fig. S5 and Table S3).

Although even after treatment, it seems both the open-circuit voltage and the short-circuit current density are rather small. We consider that another tempting direction to further improve the energy conversion efficiency is to construct an efficient p-type sensitizer. Recently, Wang huan et al. have reported that p-type DSSCs based on organometal halide perovskite-sensitized NiO have gained an enhancing short current density (9.47 mA/cm^2) and efficiency (0.71 %)[41]. If p-type semiconductor is be adopted in a working solar cells with both a photoanode and a photocathode, the optimized NiO surface and using efficient p-type sensitizers are both necessary to further improve the performance.

4. Conclusion

In this present work, we provided a good understanding of the surface chemistries, surface composition, interfacial energetics and kinetics of bare and post-treated NiO films, combining the results of the XPS, MS and EIS. The results will help us to elucidate the relativity between complex surface chemistries of NiO photocathode and kinetics of photoelectrochemical process occurring in solar energy-related devices. The study herein shows that more NiO(OH) species on the NiO film surface can be introduced by the UV-ozone post-treatment, while the surface Ni^{3+} species (e.g. NiO(OH) structure) obviously reduced by additional thermal treatment. Mott-Schottky measurements demonstrate the more dipolar NiO(OH) species form,

the more acceptor density exist in the NiO film. Moreover, the more dipolar NiO(OH) species added through UV-ozone treatment lead to an obvious negative movement of E_{fb}. Other remarkable result was NiO photocathode has deeper trap states energy distribution than those of n-type DSSCs, as result bringing about more serious charge recombination problems, which proved that understating and controlling NiO surface and/or interface structure is dominant factor of the photovoltaic devices performance. Furthermore, EIS analysis reflects that NiO(OH) species act as recombination center, and as result worsening interface recombination. Thus, modified NiO photocathode with less surface defect species, especially the NiO(OH) structure, can be predicted to result excellent photovoltaic performance. We also offer an effective way of reduction surface NiO(OH) structure by $Ni(CH_3COOH)_2$ post-treatment method, resulting in a 31.3% increased photovoltaic performance.

Acknowledgments

The authors acknowledge the supports of National Natural Science Foundation of China (51302164, 51472154, 51202138 and 51202140), Natural Science Foundation of Shanghai (13ZR1417100, 12ZR1410500). Shanghai Municipal Science and Technology Commission (13DZ2292100), Baoshan District Science and Technology Commission of Shanghai (bkw2013142), Professional and Technical Service Platform for Designing and Manufacturing of Advanced Composite Materials, Shanghai.

Notes and references

1. F. Odobel, Y. Pellegrin, E. A. Gibson, A. Hagfeldt, A. L. Smeigh and L. Hammarström, *Coordination Chemistry Reviews*, 2012, **256**, 2414-2423.
2. F. Odobel, L. Le Pleux, Y. Pellegrin and E. Blart, *Acc. Chem. Res.*, 2010, **43**, 1063-1071.
3. F. Odobel and Y. Pellegrin, *J. Phys. Chem. Lett.*, 2013, **4**, 2551-2564.
4. H. T. Nguyen, H. Jeong, J. Y. Park, Y. H. Ahn and S. Lee, *ACS Appl. Mater. Interfaces*, 2014, **6**, 7286-7291.
5. Z. L. Zhu, Y. Bai, T. Zhang, Z. K. Liu, X. Long, Z. H. Wei, Z. L. Wang, L. X. Zhang, J. N. Wang, F. Yan and S. H. Yang, *Angew. Chem. Int. Ed.*, 2014, **53**, 12571-12575.
6. S. Y. Liu, R. Liu, Y. Chen, S. H. Ho, J. H. Kim and F. So, *Chem. Mater.*, 2014, **26**, 4528-4534.
7. C. J. Flynn, E. E. Oh, S. M. McCullough, R. W. Call, C. L. Donley, R. Lopez and J. F. Cahoon, *J. Phys. Chem. C*, 2014, **118**, 14177-14184.
8. D. Y. Ma, G. Y. Shi, H. Z. Wang, Q. H. Zhang and Y. G. Li, *J. Mater. Chem. A*, 2014, **2**, 13541-13549.
9. H. Huang, J. Tian, W. K. Zhang, Y. P. Gan, X. Y. Tao, X. H. Xia and J. P. Tu, *Electrochimica Acta*, 2011, **56**, 4281-4286.
10. C. Hu, K. Chu, Y. Zhao and W. Y. Teoh, *ACS Appl. Mater. Interfaces*, 2014, **6**, 18558-18568.
11. K. Fominykh, J. M. Feckl, J. Sicklinger, M. Döblinger, S. Böcklein, J. Ziegler, L. Peter, J. Rathousky, E.-W. Scheidt, T. Bein and D. Fattakhova-Rohlfing, *Advanced Functional Materials*, 2014, **24**, 3123-3129.
12. A. Bachmeier, S. Hall, S. W. Ragsdale and F. A. Armstrong, *J. Am. Chem. Soc.*, 2014, **136**, 13518-13521.
13. J. W. Wan, G. J. Fang, P. L. Qin, Q. Zheng, N. S. Liu, N. H. Sun, Y. Tu, X. Fan, F. Cheng and X. Z. Zhao, *Sol. Energy Mater. Sol. Cells*, 2012, **101**, 289-294.
14. K. C. Wang, P. S. Shen, M. H. Li, S. Chen, M. W. Lin, P. Chen and T. F. Guo,

ACS Appl. Mater. Interfaces, 2014, **6**, 11851-11858.

15. L. D'Amario, G. Boschloo, A. Hagfeldt and L. Hammarstrom, *J. Phys. Chem. C*, 2014, **118**, 19556-19564.
16. E. L. Ratcliff, J. Meyer, K. X. Steirer, A. Garcia, J. J. Berry, D. S. Ginley, D. C. Olson, A. Kahn and N. R. Armstrong, *Chem. Mater.*, 2011, **23**, 4988-5000.
17. Z. Y. Wang, S. H. Lee, D. H. Kim, J. H. Kim and J. G. Park, *Sol. Energy Mater. Sol. Cells*, 2010, **94**, 1591-1596.
18. M. T. Greiner, M. G. Helander, Z. B. Wang, W. M. Tang and Z. H. Lu, *J. Phys. Chem. C*, 2010, **114**, 19777-19781.
19. F. Wang, G. Sun, C. Li, J. Liu, S. Hu, H. Zheng, Z. a. Tan and Y. Li, *ACS Appl. Mater. Interfaces*, 2014, **6**, 9458-9465.
20. S. Liu, R. Liu, Y. Chen, S. Ho, J. H. Kim and F. So, *Chem. Mater.*, 2014, **26**, 4528-4534.
21. S. Sumikura, S. Mori, S. Shimizu, H. Usami and E. Suzuki, *Journal of Photochemistry and Photobiology A: Chemistry*, 2008, **199**, 1-7.
22. D. Vlachos, M. Kamaratos and S. D. Foulias, *Journal of Physics-Condensed Matter*, 2006, **18**, 6997-7011.
23. M. A. Peck and M. A. Langell, *Chem. Mater.*, 2012, **24**, 4483-4490.
24. A. G. Marrani, V. Novelli, S. Sheehan, D. P. Dowling and D. Dini, *ACS Appl. Mater. Interfaces*, 2014, **6**, 143-152.
25. Y. Fang, X. Ai, X. Wang, Q. Wang, J. Huang and T. Wu, *J. Alloys Compd.*, 2014, **594**, 211-216.
26. E. Thimsen, A. B. F. Martinson, J. W. Elam and M. J. Pellin, *J. Phys. Chem. C*, 2012, **116**, 16830-16840.
27. A. Renaud, B. Chavillon, L. Le Pleux, Y. Pellegrin, E. Blart, M. Boujtita, T. Pauporte, L. Cario, S. Jobic and F. Odobel, *J. Mater. Chem.*, 2012, **22**, 14353-14356.
28. Z. Ji, G. Natu, Z. Huang, O. Kokhan, X. Zhang and Y. Wu, *J. Phys. Chem. C*, 2012, **116**, 16854-16863.

29. Z. Huang, G. Natu, Z. Ji, M. He, M. Yu and Y. Wu, *The Journal of Physical Chemistry C*, 2012, **116**, 26239-26246.

30. H. Yang, G. H. Guai, C. Guo, Q. Song, S. P. Jiang, Y. Wang, W. Zhang and C. M. Li, *J. Phys. Chem. C*, 2011, **115**, 12209-12215.

31. L. Peter, *Acc. Chem. Res.*, 2009, **42**, 1839-1847.

32. M. S. Góes, E. Joanni, E. C. Muniz, R. Savu, T. R. Habeck, P. R. Bueno and F. Fabregat-Santiago, *J. Phys. Chem. C*, 2012, **116**, 12415-12421.

33. Q. Wang, S. Ito, M. Grätzel, F. Fabregat-Santiago, I. Mora-Seró, J. Bisquert, T. Bessho and H. Imai, *J. Phys. Chem. B*, 2006, **110**, 25210-25221.

34. L. M. Peter, *J. Phys. Chem. C*, 2007, **111**, 6601-6612.

35. Y. Kusumawati, M. A. Martoprawiro and T. Pauporté, *J. Phys. Chem. C*, 2014, **118**, 9974-9981.

36. G. Natu, Z. Huang, Z. Ji and Y. Wu, *Langmuir : the ACS journal of surfaces and colloids*, 2012, **28**, 950-956.

37. S. Uehara, S. Sumikura, E. Suzuki and S. Mori, *Energy & Environmental Science*, 2010, **3**, 641.

38. T. A. Peiris, J. S. Sagu, K. G. Wijayantha and J. Garcia-Canadas, *ACS applied materials & interfaces*, 2014, **6**, 14988-14993.

39. X. Dou, D. Sabba, N. Mathews, L. H. Wong, Y. M. Lam and S. Mhaisalkar, *Chemistry of Materials*, 2011, **23**, 3938-3945.

40. K.-C. Wang, P.-S. Shen, M.-H. Li, S. Chen, M.-W. Lin, P. Chen and T.-F. Guo, *ACS Appl. Mater. Interfaces*, 2014, **6**, 11851-11858.

41. H. Wang, X. Zeng, Z. Huang, W. Zhang, X. Qiao, B. Hu, X. Zou, M. Wang, Y.-B. Cheng and W. Chen, *ACS applied materials & interfaces*, 2014, **6**, 12609-12617.

42. L. Berkat, L. Cattin, A. Reguig, M. Regragui and J. C. Bernede, *Mater. Chem. Phys.*, 2005, **89**, 11-20.

43. D. T. Nguyen, A. Ferrec, J. Keraudy, M. Richard-Plouet, A. Goullet, L. Cattin, L. Brohan and P. Y. Jouan, *Surf. Coat. Technol.*, 2014, **250**, 21-25.

44. A. Renaud, B. Chavillon, L. Cario, L. L. Pleux, N. Szuwarski, Y. Pellegrin, E. Blart, E. Gautron, F. Odobel and S. Jobic, *The Journal of Physical Chemistry C*, 2013, **117**, 22478-22483.

45. A. P. Grosvenor, M. C. Biesinger, R. S. Smart and N. S. McIntyre, *Surf. Sci.*, 2006, **600**, 1771-1779.

Tables and Fig. captions

Table 1. Surface analysis by XPS spectra for the bare and post-treatment NiO.

Table 2. Values of acceptor-state densities, apparent flat-band potentials for bare and post-treated NiO Films.

Fig. 1. Ni 2p spectra for NiO films, form bottom to top: (a) NiO, (b) NiO-S and (c) NiO-ozone. Raw data is given by (●) and with fitted components (orange lines).

Fig. 2. O 1s spectra for NiO films, form bottom to top: (a) NiO, (b) NiO-S and (c) NiO-ozone. Raw data is given by (●) and with fitted components (orange lines).

Fig. 3. Mott-Schottky polts for NiO, NiO-S, and NiO-ozone films against an aqueous electrolyte containing 0.1 M PB (0.2 M NH_2PO_4, 0.2M Na_2HPO_4), 1 M KCl, and pH adjusted to 7.0.

Fig. 4. (A) Bode plots and (B) Nyqusit plots of p-type DSSCs employing NiO, NiO-S and NiO-ozone films at 60 mV bias in the dark.

Fig. 5. (A) chemical capacitance, (B) Hole recombination resistance, hole transport resistance, (C) Hole liftetime , hole transport time and (D) collection efficiency of device employing bare and post-treatment NiO photocathodes as a function of corrected voltage obtained from impedance spectra (sample NiO: black, sample NiO-S: red and sample NiO-ozone : blue).

Fig. 6. Current-voltage characteristics of NiO, NiO-S and NiO-ozone devices understandardized AM 1.5 illumination of 100 mW/cm^2 (active area 0.25 cm^2).

Table 1. Surface analysis by XPS spectra for the bare and post-treatment NiO

	O1s			Ni $2p_{3/2}$			
sample	NiO (529)[a] [eV]	$Ni(OH)_2$ (530.7~531.3)[a] [eV]	NiOOH (532)[a] [eV]	NiO (853.7~854.1)[b] [eV]	$Ni(OH)_2$ (854.9~855.6)[b] [eV]	NiOOH (856.4)[b] [eV]	(NiO:$Ni(OH)_2$:NiOOH)[c]
NiO	529.23	530.93	-	853.68	855.13	856.00	1:2.15:1.03
NiO-S	529.00	530.76	-	853.44	855.14	-	1:3.44:-[d]
NiO-ozone	529.39	530.87	532.33	853.83	855.13	856.01	1:2.29:1.47

[a] The peak position for O 1s obtained by literature.[42, 43]

[b] The peak position for Ni $2p_{3/2}$ obtained by literature.[16, 44, 45]

[c] The percentage composition of NiOOH was calculated from Ni $2p_{3/2}$ fitting data.

[d] The radio is the value of NiO:$Ni(OH)_2$.

Table 2. Values of acceptor-state densities and apparent flat-band potentials for bare and post-treated NiO films

Sample	N_A [$\times 10^{18}$/cm^3]	E_{fb} [V vs NHE]
NiO	7.75	0.40
NiO-S	7.56	0.44
NiO-ozone	8.44	0.38

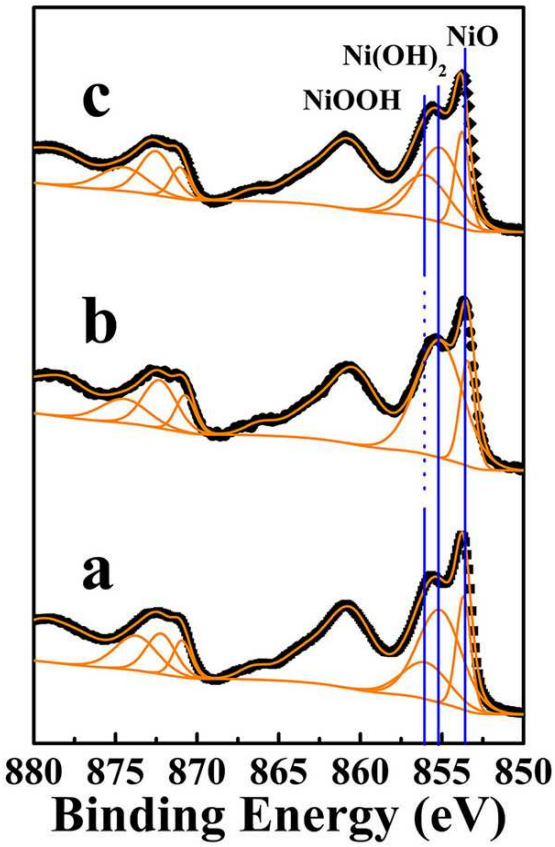

Fig. 1. Ni 2p spectra for NiO films, form bottom to top: (a) NiO, (b) NiO-S and (c) NiO-ozone. Raw data is given by (●) and with fitted components (orange lines).

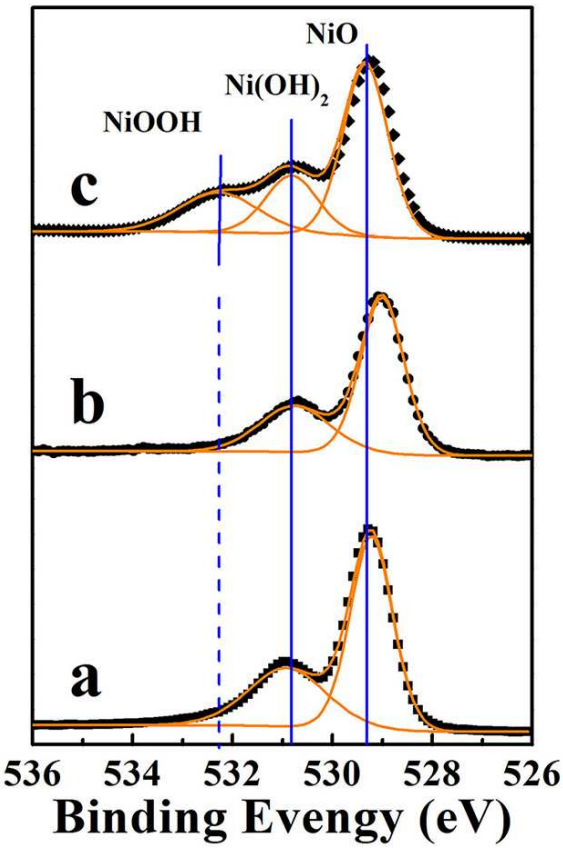

Fig. 2. O 1s spectra for NiO films, form bottom to top: (a) NiO, (b) NiO-S and (c) NiO-ozone. Raw data is given by (●) and with fitted components (orange lines).

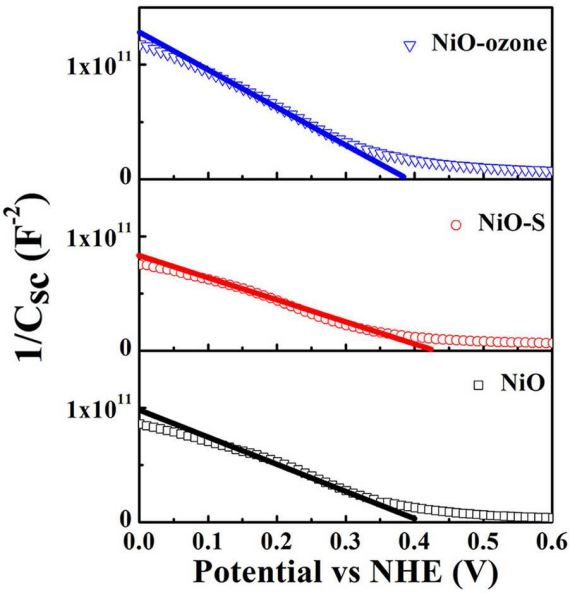

Fig. 3. Mott-Schottky polts for NiO, NiO-S, and NiO-ozone films against an aqueous electrolyte containing 0.1 M PB (0.2 M NH_2PO_4, 0.2M Na_2HPO_4), 1 M KCl, and pH adjusted to 7.0.

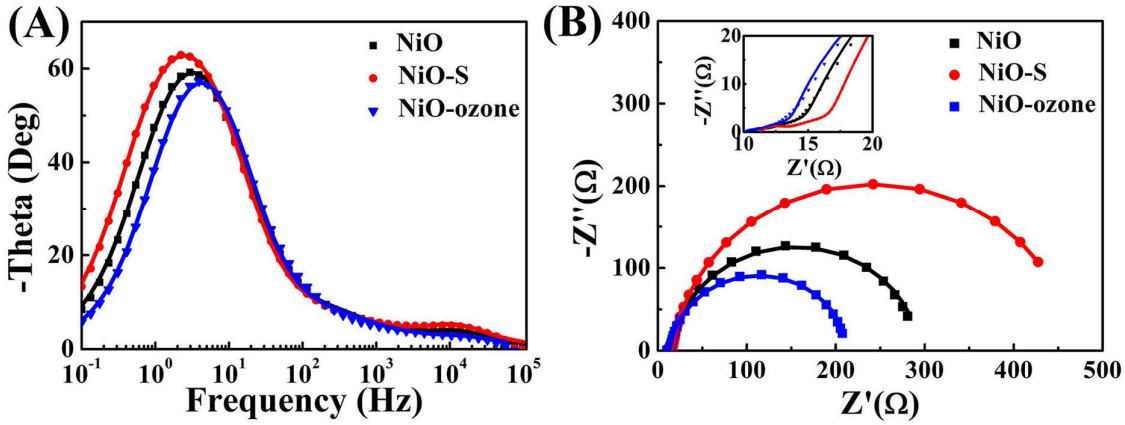

Fig. 4. (A) Bode plots and (B) Nyqusit plots of p-type DSSCs employing NiO, NiO-S and NiO-ozone films at 60 mV bias in the dark.

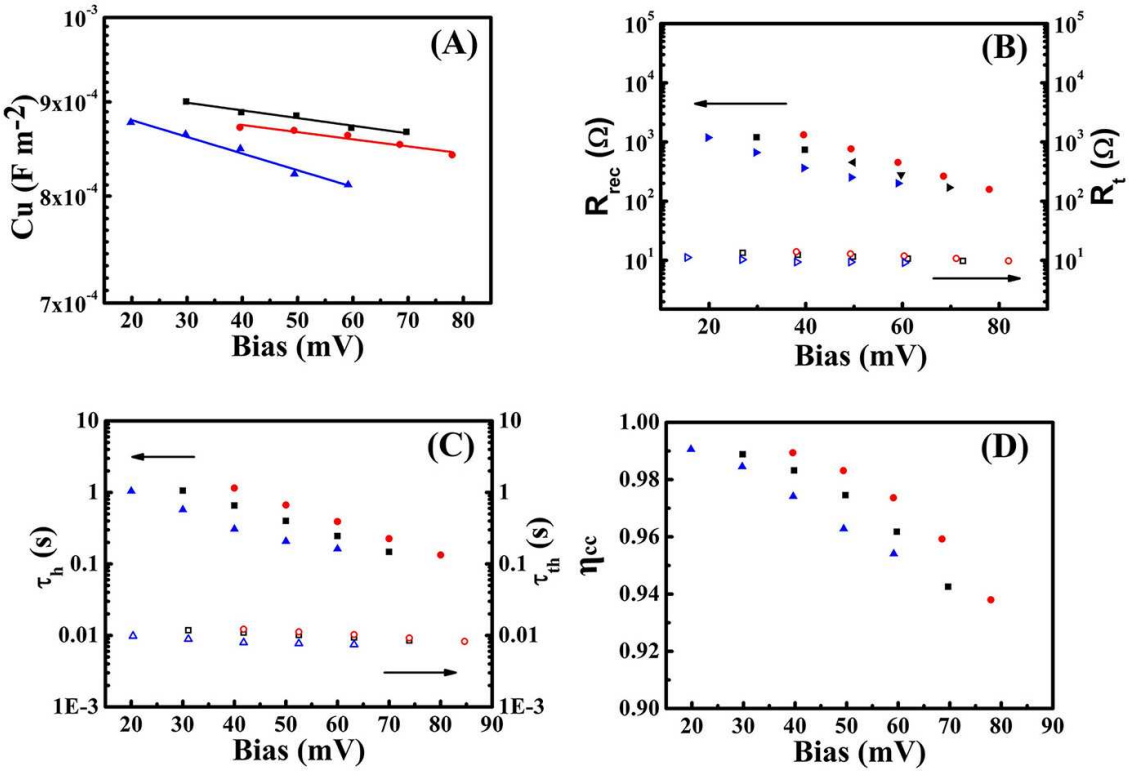

Fig. 5. (A) chemical capacitance, (B) Hole recombination resistance, hole transport resistance, (C) Hole liftetime , hole transport time and (D) collection efficiency of device employing bare and post-treatment NiO photocathodes as a function of corrected voltage obtained from impedance spectra (sample NiO: black, sample NiO-S: red and sample NiO-ozone : blue).

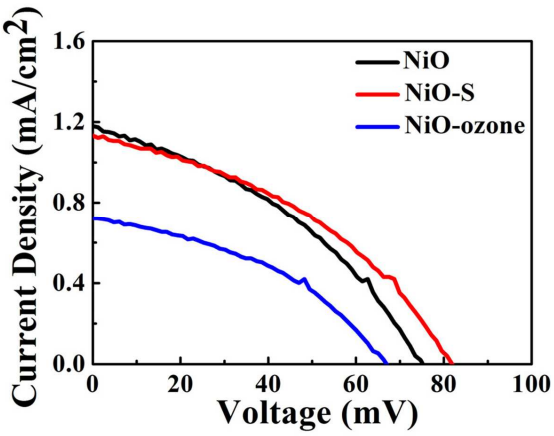

Fig. 6. Current-voltage characteristics of NiO, NiO-S and NiO-ozone devices under standardized AM 1.5 illumination of 100 mW/cm^2 (active area 0.25 cm^2).

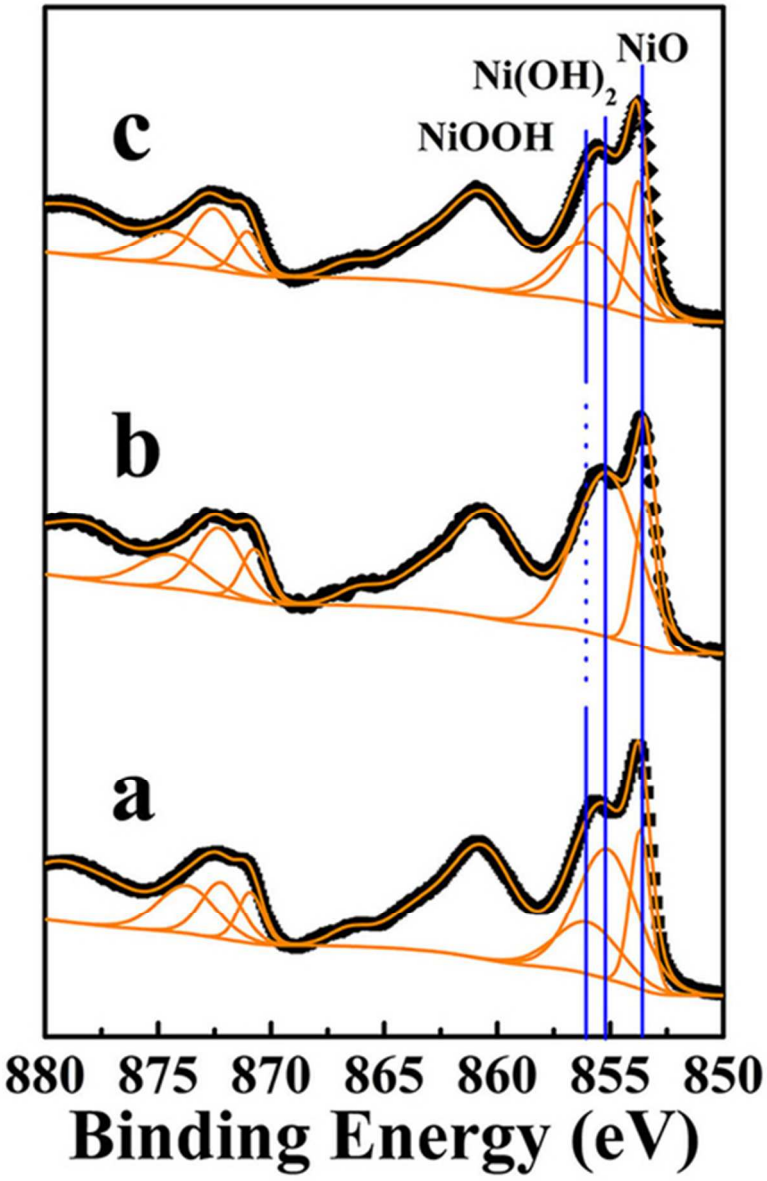

39x60mm (300 x 300 DPI)

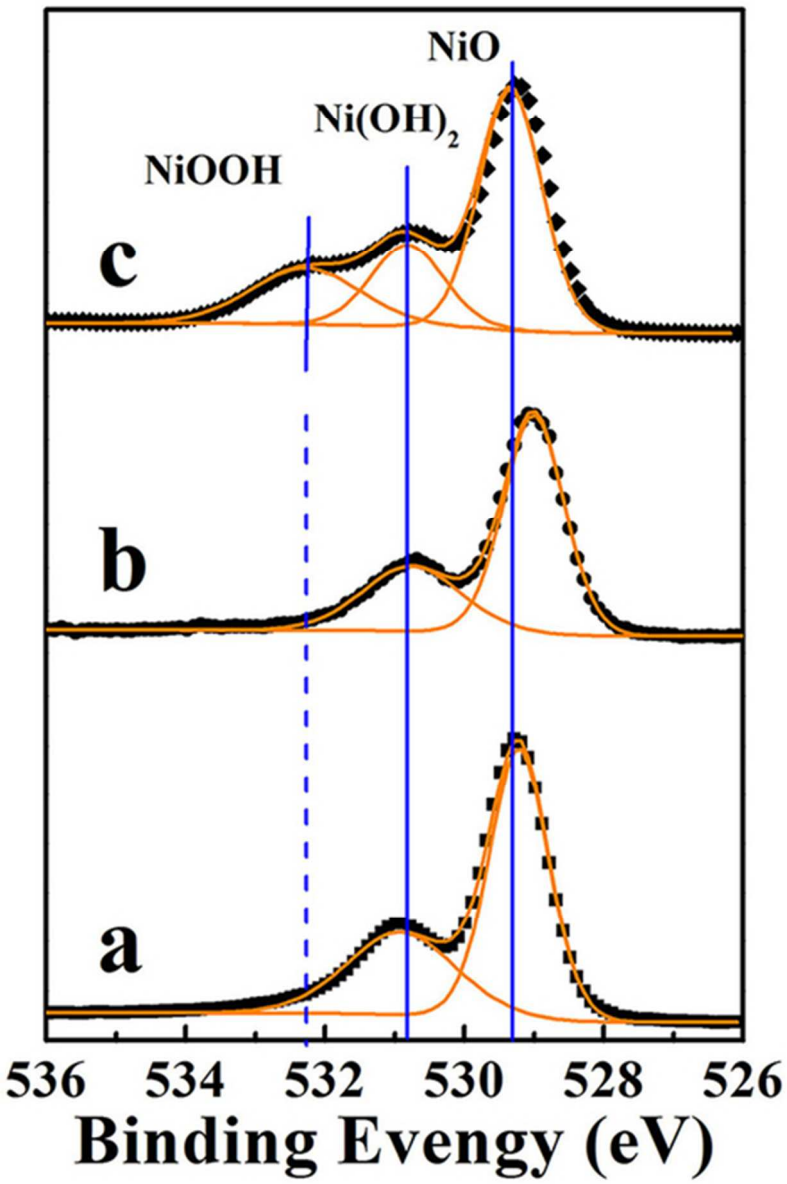

39x60mm (300 x 300 DPI)

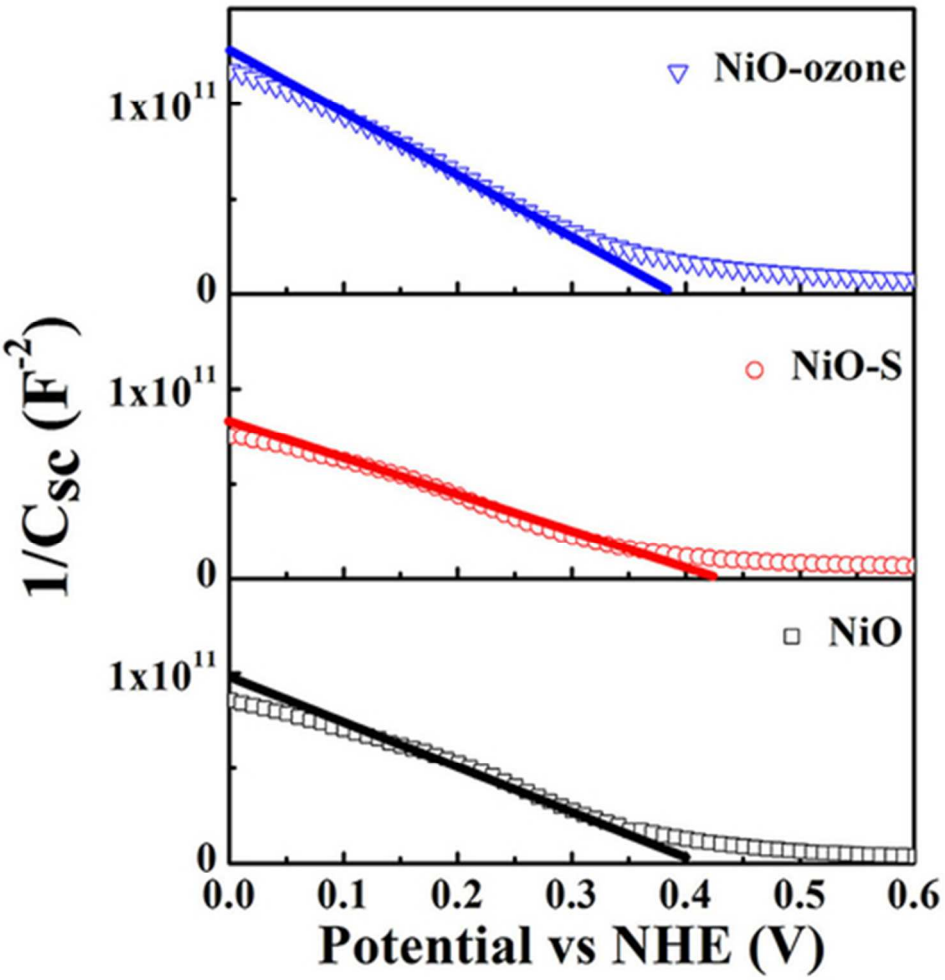

39x41mm (300 x 300 DPI)

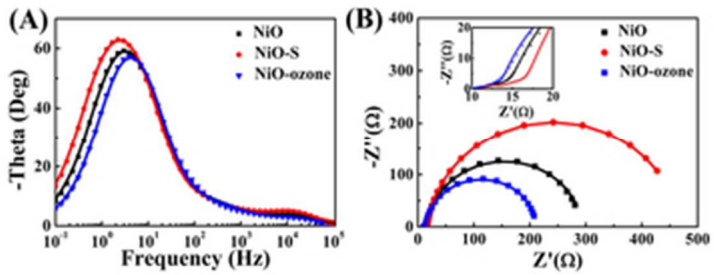

30x11mm (300 x 300 DPI)

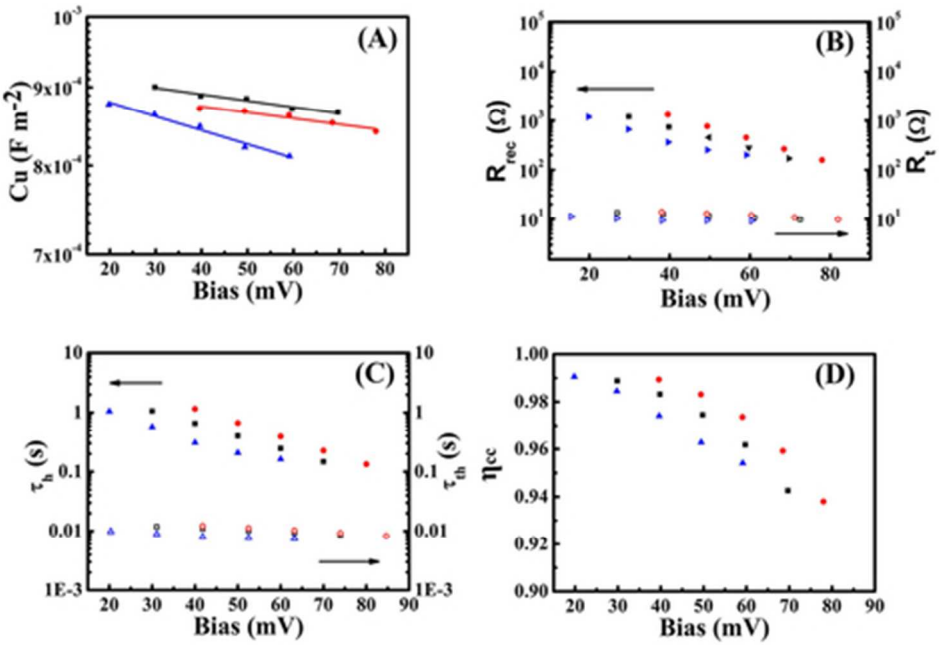

39x27mm (300 x 300 DPI)

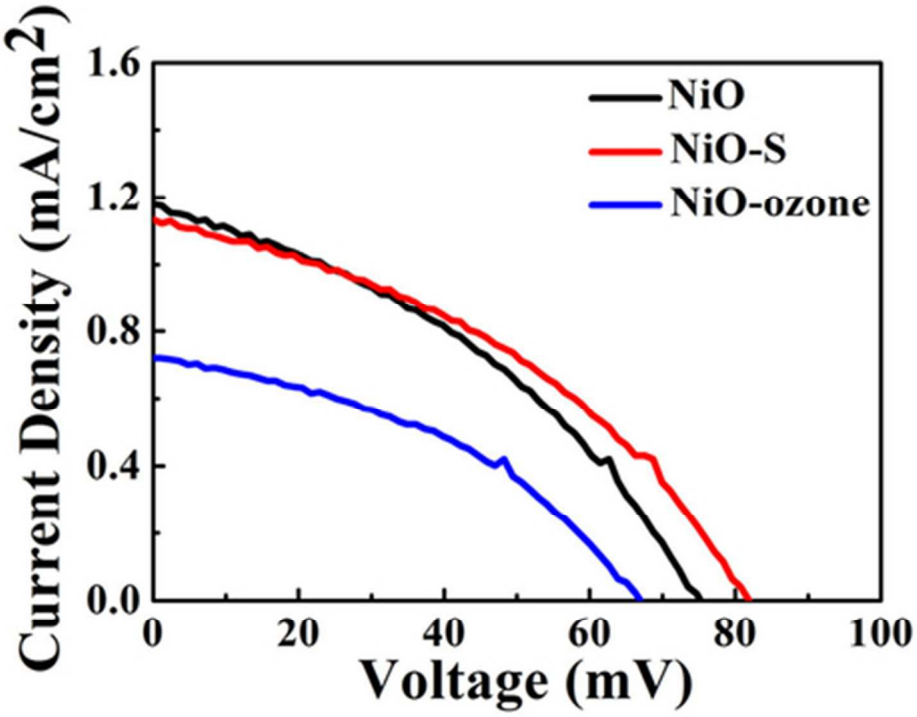

39x31mm (300 x 300 DPI)

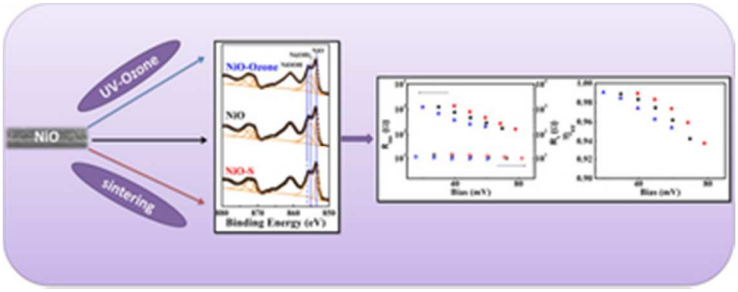

30x12mm (300 x 300 DPI)